

Geophysical Research Letters

Supporting Information for

Extraction of mantle discontinuities from teleseismic ambient noise

Shota Kato¹ and Kiwamu Nishida¹

¹Earthquake Research Institute, the University of Tokyo

Contents of this file

Supplementary Text 1
Figures S1 to S6

Text S1.

Calculation method of gRFs (PKIKP events)

The calculation method of gRFs of PKIKP events was modified from the original calculation method due to the coherent instrumental noise (Takagi *et al.*, 2015). Because the travel time of PKIKP is almost the same within the array, the noise would be coherently stacked in the estimated P-wave source time function. To suppress the noise, we used a different waveform between the successive-day alternative to the original waveform (Takagi *et al.*, 2020).

Figure S1.

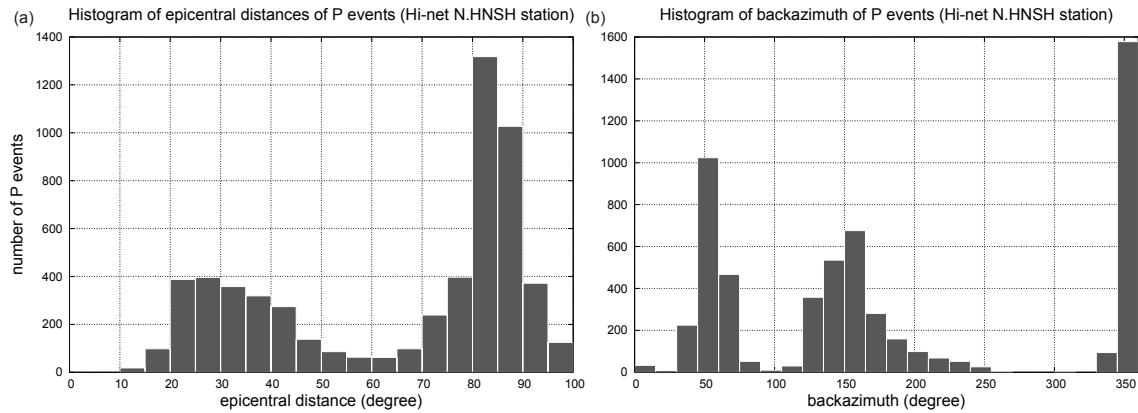


Figure S1. Histogram of epicentral distance (a) and back azimuth (b) of P-wave microseisms at N.HNSH station (34.7283° N 134.2744° E, Okayama Prefecture, Japan) of Hi-net. (a) The peak at $20-45^{\circ}$ is the P-wave microseisms at the Northern Pacific Ocean, whereas the peak at $80-90^{\circ}$ is the P-wave microseisms at the Northern Atlantic and Southern Pacific Ocean. (b) The peak at the $45-75^{\circ}$, $120-180^{\circ}$, and $345-360^{\circ}$ is the P-wave microseisms at the Northern Pacific, Southern Pacific, and Northern Atlantic Ocean, respectively.

Figure S2.

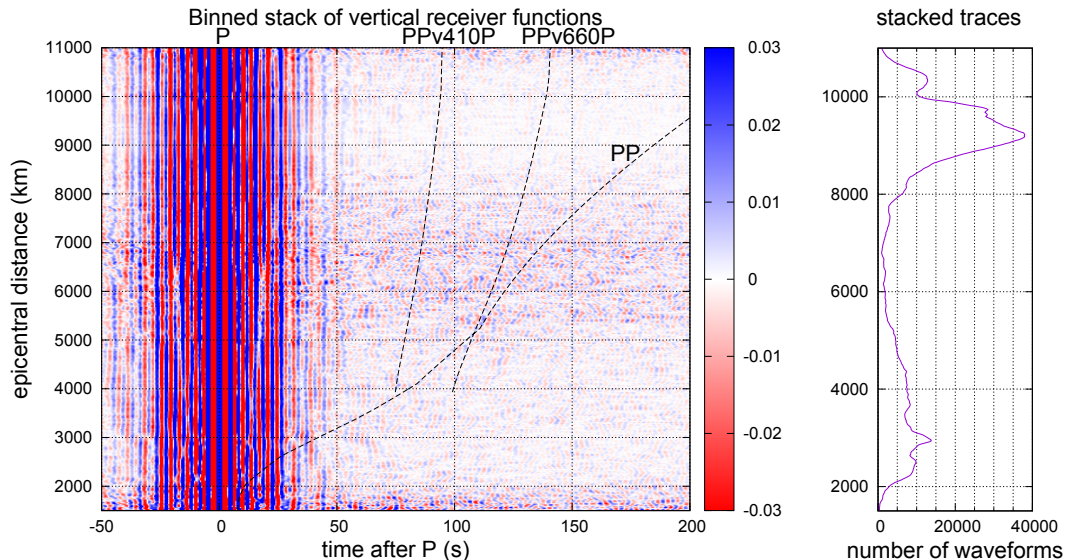


Figure S2. Binned stack of vertical gRFs of P events. Three black lines show the theoretical travel time of PP, PP410P, and PP660P from AK135 (Kennett *et al.*, 1995). These phases are not clear even if the color range is set to narrow.

Figure S3.

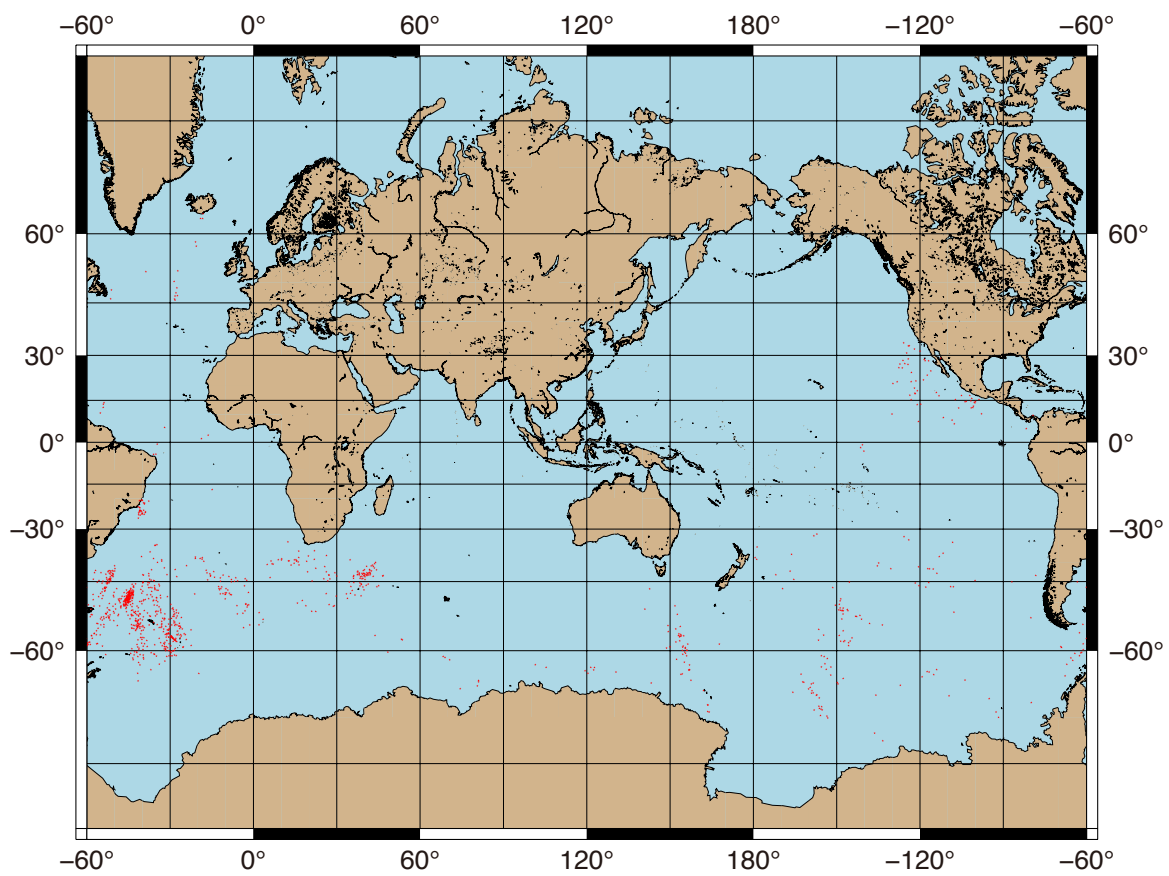


Figure S3: Centroid distribution of P-wave microseisms (PP phase) used in this study. Red dots denote 1123 P wave source locations (Nishida & Takagi, 2022).

Figure S4.

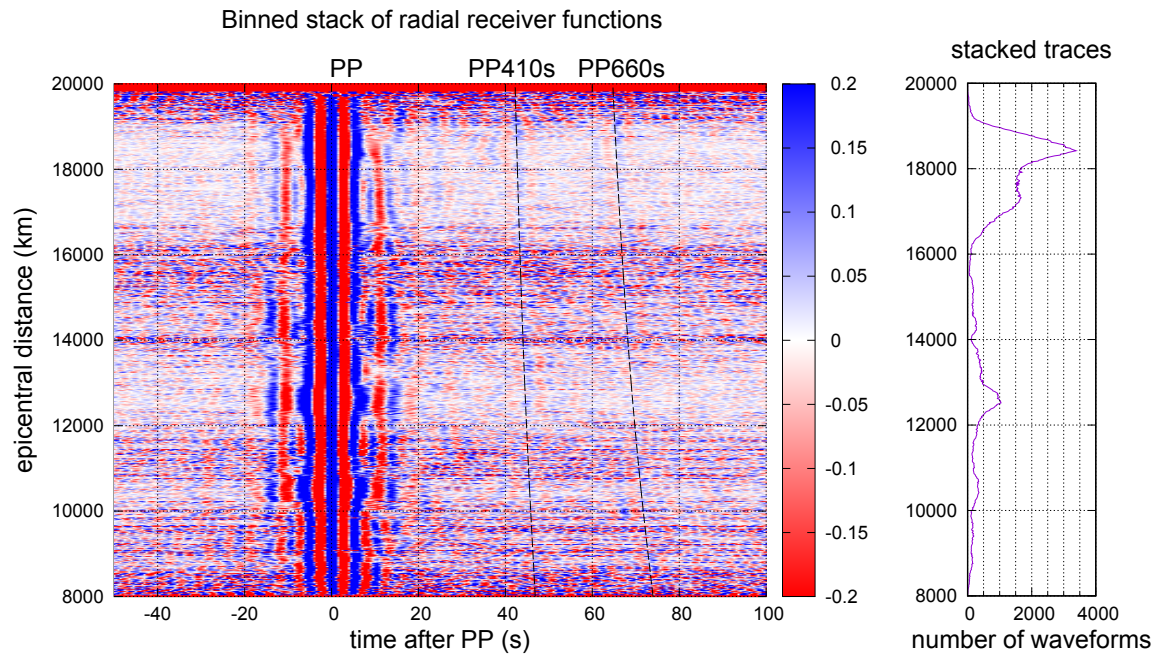


Figure S4. Binned stack of radial gRFs of PP events. This shows the P-s converted waves at the mantle discontinuities (PP410s/PP660s) with an epicentral distance of 12,000-19,000 km. The relative arrival time of these waves were consistent with the theoretical travel times of AK135, although these waves are less clear than P-s waves in P events.

Figure S5.

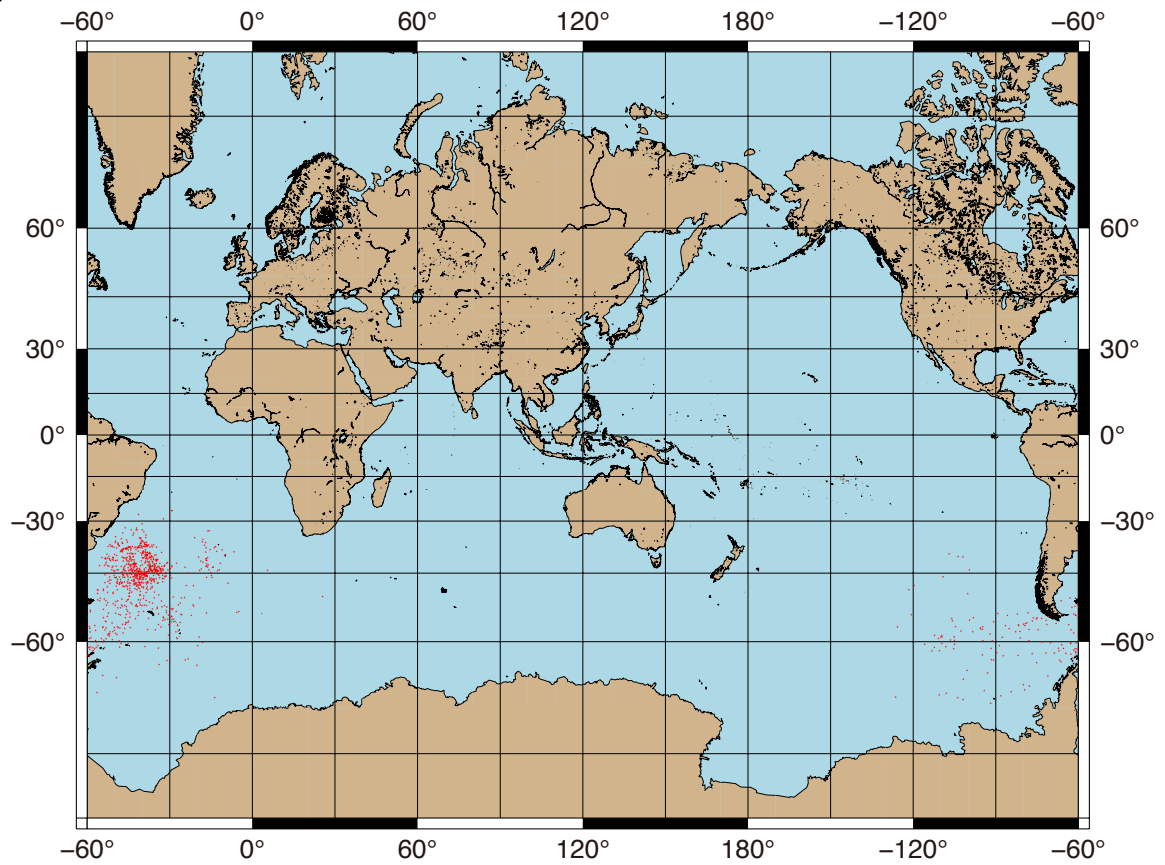


Figure S5: Centroid distribution of P-wave microseisms (PKIKP phase) used in this study. Red dots denote 997 P wave source locations (Nishida & Takagi, 2022).

Figure S6.

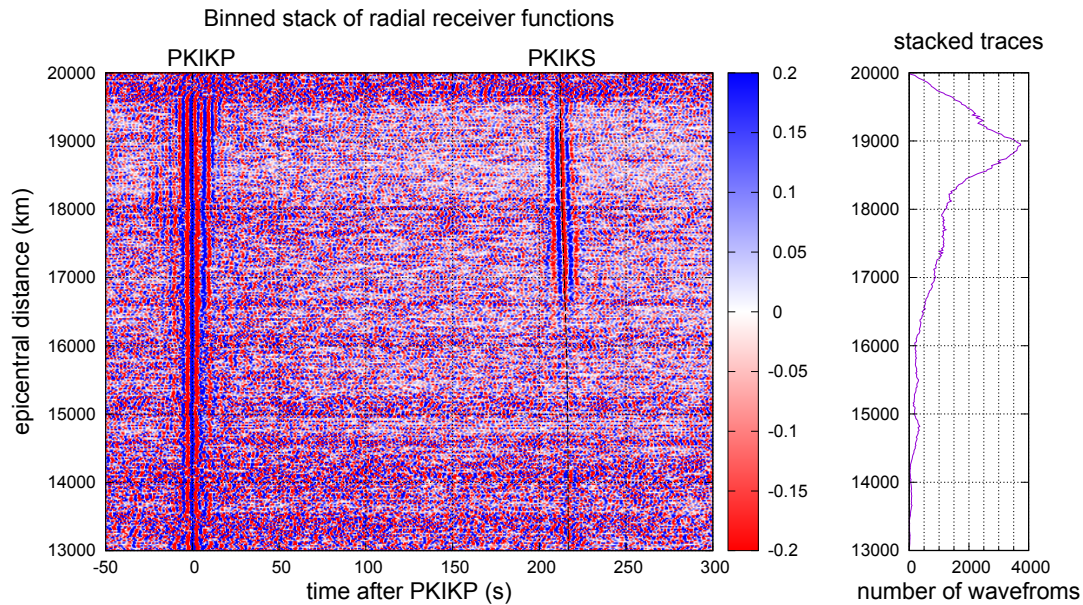


Figure S6. Binned stack of radial gRFs of PKIKP events. This shows the PKIKS, P-s converted at the core-mantle boundary, with an epicentral distance of 17,000-19,000 km (Liu & Shearer, 2022).

Reference:

- Kennett, B. L. N., Engdahl, E. R., & Buland, R. (1995). Constraints on seismic velocities in the Earth from traveltimes. *Geophysical Journal International*, 122(1), 108–124.
- Liu, T., & Shearer, P. M. (2022). Likely P - to - S conversion at the core - mantle boundary extracted from array processing of noise records. *Geophysical Research Letters*, 49(7).
- Nishida, K., & Takagi, R. (2022). A Global Centroid Single Force Catalog of P-Wave Microseisms. *Journal of Geophysical Research*, [Solid Earth], 127(4), e2021JB023484.
- Takagi, R., Nishida, K., Aoki, Y., Maeda, T., Masuda, K., Takeo, M., et al. (2015). A Single Bit Matters: Coherent Noise of Seismic Data Loggers. *Seismological Research Letters*, 86(3), 901–907.
- Takagi, R., Toyokuni, G., & Chikasada, N. (2020). Ambient noise correlation analysis of S-net records: extracting surface wave signals below instrument noise levels. *Geophysical Journal International*, 224(3), 1640–1657.